Inorganic Chemistry

Article

pubs.acs.org/IC

Iridium(III) Emitters Based on 1,4-Disubstituted-1*H*-1,2,3-triazoles as Cyclometalating Ligand: Synthesis, Characterization, and Electroluminescent Devices

Jesús M. Fernández-Hernández,*[,†] Juan I. Beltrán,[‡] Vincent Lemaur,[‡] Maria-Dolores Gálvez-López,[†] Chen-Han Chien,[†] Federico Polo,[†] Enrico Orselli,[§] Roland Fröhlich,[∥] Jérôme Cornil,*[,‡] and Luisa De Cola*[,†,⊥]

[†]Physikalisches Institut, Center for Nanotechnology (CeNTech), Westfälische Wilhelms-Universität Münster, Heisenbergstrasse 11, 48149 Münster, Germany

[‡]Service de Chimie des Matériaux Nouveaux, Université de Mons, Place du Parc 20, 7000 Mons, Belgium

[§]Solvay S. A., Rue de Ransbeek 310, 1120 Brussels, Belgium

[∥]Organisch-Chemisches Institut, Westfälische Wilhelms-Universität Münster, Corrensstrasse 40, 48149 Münster, Germany

Supporting Information

ABSTRACT: A series of blue and blue-green emitters based on neutral bis- and tris-cyclometalated Ir(III) complexes with 1-benzyl-4-(2,6-difluorophenyl)-1*H*-1,2,3-triazole (dfptrBn) as cyclometalating ligand is reported. The bis-cyclometalated complexes of the type $[Ir(dfptrBn)_2(L\text{^}X)]$ with different ancillary ligands, L^X = picolinate (pic) (**2**) or 2-(5-(perfluorophenyl)-2*H*-1,2,4-triazol-3-yl)pyridine ($pytrF_5$) (**3**), are described and their photophysical properties compared with the analogous complexes containing the archetypal 2-(2,4-difluorophenyl)-pyridinato (dfppy) as cyclometaled ligand (C^N). Complex **2** exhibits a marked solvatochromic behavior, from 475 nm in toluene to 534 nm in formamide, due to the strong MLCT character of its emissive excited state. Complex **3** displays a true-blue emission, narrower in the visible part than FIrpic. In addition, the homoleptic complex $[Ir(dfprBn)_3]$ (**4**) and the heteroleptic compounds with mixed arylpyridine/aryltriazole ligands, $[Ir(dfptrBn)_2(C\text{^}N)]$ (C^N = 2-phenylpyridinato (ppy) (**5**) or dfppy (**6**)), have been synthesized and fully characterized. The facial (*fac*) complex ***fac*-4** is emissive at 77 K showing a deep-blue emission, but it is not luminescent in solution at room temperature similarly to their phenylpyrazole counterparts. However, the *fac* isomers, ***fac*-5** and ***fac*-6**, are highly emissive in solution and thin films, reaching emission quantum yields of 76%, with emission colors in the blue to blue-green region. The photophysical properties for all complexes have been rationalized by means of quantum-chemical calculations. In addition, we constructed electroluminescent devices, organic light-emitting diodes (OLEDs) by sublimation of ***fac*-6**, and by solution processed polymer-based devices (PLEDs) using complexes ***fac*-5** or ***fac*-6** as dopants.

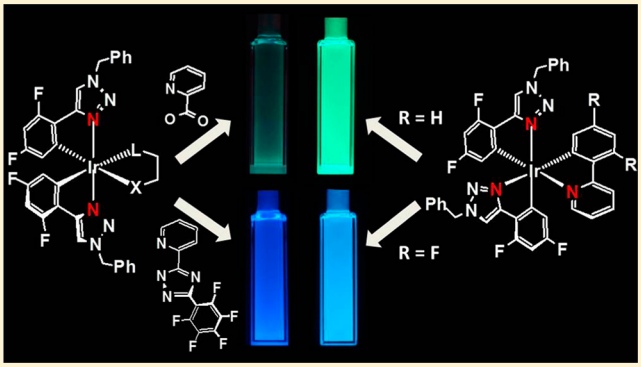

INTRODUCTION

In recent years, increasing interest has been devoted to phosphorescent metal complexes and their application as emitters in electroluminescent devices, i.e., organic light-emitting diodes (OLEDs) or light-emitting electrochemical cells (LEECs) for displays and lighting applications.[1−9] Luminescent complexes are generally based on heavy metals such as ruthenium(II), osmium(II),[10−12] platinum(II),[11,13−18] copper(I),[19−25] or iridium(III). Compounds based on iridium are the most studied among them[1−9,26,27] due to their relatively short excited-state lifetime, high emission quantum yield, and facile color tuning through ligand structure control.[1,28−30] The triplet character of the emission, induced by the strong spin−orbit coupling in these complexes, is of great importance, since it allows for harvesting of both the singlet and the triplet excitons produced when electrons and holes recombine, reaching up to 100% internal efficiency.[1,30,31] In order to develop full-color display and lighting technologies, a key factor is employment of molecules that can emit the primary colors (red, green, and blue). Cyclometalated Ir(III) complexes possess color of the emission in the visible range (from red to blue) dictated by careful design of the structure and nature of the ligands bound to the metal center.[11,29,32] Although efficient red- and green-emitting Ir(III) complexes have been described and are now in the commercialization phase due to their

Received: August 22, 2012
Published: February 5, 2013

   dx.doi.org/10.1021/ic3018419 | *Inorg. Chem.* 2013, 52, 1812−1824

excellent stability in devices, finding stable and efficient blue emitters is still an issue.[11,33−36]

Among the cyclometalating ligands employed to prepare Ir(III) complexes, the most widely used are those in which a carbon from a phenyl ring acts as a donor and the adjacent fragment involved in formation of the metallocycle is an N-heterocycle ring.[11] These ligands are represented by C^N, with 2-phenylpyridine (ppyH) as the archetypical example. These cyclometalating ligands are anionic and form a strong bond with the metal, yielding a highly stabilized ligand field that increases the splitting of d−d orbitals compared to complexes with only neutral diimine ligands.[29] Thus, the photophysical properties of these complexes are often remarkable, leading to highly luminescent organometallic compounds.[36] Furthermore, the C^N ligand can be easily substituted with electron-withdrawing or -donating groups, and these substitutions have an important effect on their HOMO and LUMO energies and consequently on the metal complex emission. In order to obtain blue emitters, several strategies can be followed. Incorporation of electron-withdrawing groups on the aryl fragment stabilizes the HOMO, while substituting the pyridine or N-heterocycle with electron-donating groups raises the LUMO, leading to an overall increase of the energy of the emission. An alternative strategy to raise the LUMO of the complex is to change the pyridine moiety by a smaller N-heterocyclic ring that has higher reduction potentials than pyridine. Blue shifts of the emission maxima have been obtained using pyrazoles,[36−40] N-heterocyclic carbenes (NHC),[34,41−44]or triazoles. For the latter, Samuel et al. showed that 5-aryl-1,3-disubstituted-[1,2,4]-triazole can be successfully used as cyclometalating ligand to obtain bluer emitters than the arylpyridine counterparts.[45,46] An interesting alternative to the phenyl-1,2,4-triazole is the use of 1,4-disubstituted-1*H*-1,2,3-triazole. These compounds can be easily prepared by "click chemistry", which allows for wide functionalization of the aryl or triazole moieties via the acetylene or organic azide.[47,48] Recently, we and others successfully synthesized 1-substituted-4-aryl-1*H*-1,2,3-triazoles and exploited them as cyclometalating ligands in neutral and cationic Ir(III) complexes.[49−53] Although it has been shown that their emission can be blue shifted compared to their arylpyridine counterparts,[49−51,53] to the best of our knowledge, the number of neutral efficient blue or sky blue emitters based on these ligands is rather limited and their use as dopant in electroluminescent devices is rare.

Herein, we report a new class of blue and blue-green emitters based on neutral bis- and tris-cyclometalated Ir(III) complexes with 1-benzyl-4-(2,6-difluorophenyl)-1*H*-1,2,3-triazole (dfptrBn) as cyclometalating ligand. The bis-cyclometalated complexes of the type $[Ir(dfptrBn)_2(L^X)]$ with different ancillary ligands, L^X = picolinate (pic) or, $pytrF_5$, are described as well as the heteroleptic tris-cyclometalated complexes with mixed arylpyridine/aryltriazole ligands, $[Ir(dfptrBn)_2(C^N)]$ (C^N = ppy or dfppy). The properties have been investigated and compared with analogous complexes containing the archetypal dfppy as cyclometalating ligand (C^N).[54−56] We also present the synthesis and photophysical characterization of the first example of a homoleptic tris-cyclometalated complex based on 1,4-disubstituted-1*H*-1,2,3-triazole. The photophysical properties for all complexes have been rationalized by means of quantum-chemical calculations. In addition, device characteristics of polymer light-emitting diodes (PLEDs) and OLEDs doped with the tris-cyclometalated Ir(III) complexes are presented.

EXPERIMENTAL SECTION

General Information and Materials. Solvents were dried using standard procedures. All other reagents were used as received from commercial sources, unless otherwise stated. 1-Benzyl-4-(2,4-difluorophenyl)-1*H*-1,2,3-triazole (dfptrBn), 2-(5-(perfluorophenyl)-2*H*-1,2,4-triazol-3-yl)pyridine ($pytrF_5$), and dimer $[Ir_2(dfptrBn)_4Cl_2]$ (**1**) were synthesized as described elsewhere.[51,52,55,57] NMR spectra were recorded on an ARX 300 or AMX 400 from Bruker Analytische Messtechnik (Karlsruhe, Germany). ^{1}H NMR chemical shifts (δ) of the signals are given in ppm and referenced to residual protons in the deuterated solvents: $CDCl_3$ (7.26 ppm), dimethyl sulfoxide-d_6 (2.50 ppm), or CD_3CN (1.94 ppm). ^{19}F NMR chemical shifts are referenced to $CFCl_3$ (0.00 ppm) as an internal standard. Signal splittings are abbreviated as follows: s = singlet; d = doublet; t = triplet; q = quartet; m = multiplet. All coupling constants (J) are given in Hertz (Hz). Mass spectrometry was performed in the Department of Chemistry, University of Münster. Electrospray ionization (ESI) mass spectra were recorded on a Bruker Daltonics (Bremen, Germany) MicroTof with loop injection. Elemental analysis was recorded at the University of Milan, Italy.

Preparation. *$[Ir(dfptrBn)_2(pic)]$ (**2**).* To a solution of **1** (118 mg, 0.0768 mmol) in 2-ethoxyethanol (7 mL), picolinic acid (21 mg, 0.169 mmol) and sodium carbonate (80 mg, 0.754 mmol) were added. The reaction mixture was placed under inert atmosphere and refluxed for 16 h in the dark. To the cooled reaction mixture 50 mL of EtOAc was added. The mixture was washed three times with water (3 × 15 mL), and the organic phase was dried over $MgSO_4$. Crude product was purified by flash chromatography on silica gel using EtOAc as eluent. Product can be recrystallized from MeCN/Et_2O. Yield: 96 mg, (75%). ^{1}H NMR (DMSO-d_6, 300 MHz): δ 8.77 (d, J = 1.4, 1H), 8.73 (d, J = 1.4, 1H), 8.05 (m, J = 11.5, 7.8, 4.1, 2H), 7.76 (d, J = 4.9, 1H), 7.57 (ddd, J = 7.2, 5.4, 1.9, 1H), 7.47−7.16 (m, 10H), 6.81 (dd, J = 9.9, 2.2, 1H), 6.72 (m, dd, J = 9.9, 2.2, 1H), 5.74 (AB-system, 4H, CH_2), 5.57 (dd, J = 9.1, 2.2, 1H), 5.44 (dd, J = 9.0, 2.3, 1H). ^{19}F{^{1}H} NMR (282 MHz, DMSO-d_6): δ −110.22 (d, J = 7.3, 1F), −111.04 (d, J = 6.9, 1F), −111.52 (d, J = 7.3, 1F), −112.52 (d, J = 6.9, 1F). m/z (ESI-MS+): 878.1446 ($[M + Na^+]^+$). Anal. Calcd for $C_{36}H_{24}F_4IrN_7O_2$: C, 50.58; H, 2.83; N, 11.47. Found: C, 50.33; H, 2.77; N, 11.41.

*$[Ir(dfptrBn)_2(pytrF_5)]$ (**3**).* To a solution of **1** (90 mg, 0.058 mmol) in 8 mL of dichloromethane/ethanol (3:1), $pytrF_5$ (40.2 mg, 0.129 mmol) was added. The reaction mixture was placed under inert atmosphere and refluxed for 24 h in the dark. After evaporation of the solvent, the crude product was purified by flash chromatography on a silica gel column using dichloromethane/MeCN (9:1). Product can be recrystallized from dichloromethane/Et_2O. Yield: 70 mg (60%). ^{1}H NMR (300 MHz, $CDCl_3$): δ 8.50 (bs, 1H), 7.94 (d, J = 5.3, 1H), 7.88 (t, J = 7.5, 1H), 7.67−7.52 (m, 2H), 7.46−7.32 (m, 6H), 7.27 (m, 2H), 7.21−7.05 (m, 3H), 6.51−6.39 (m, 1H), 6.34 (td, J = 10.1, 2.2, 1H), 5.77 (dd, J = 8.8, 2.2, 1H), 5.66 (dd, J = 9.0, 2.2, 1H), 5.45 (m, 4H). ^{19}F{^{1}H} NMR (282 MHz, $CDCl_3$): δ −109.32 (bs, 1F), −109.83 (bs, 1F), −111.90 (bs, 1F), −112.78 (bs, 1F), −138.66 (m, 2F), −154.22 to −156.71 (m, 2F), −163.08 (m, 2F). m/z (ESI-MS+): found 1067.155 ($[M + Na^+]^+$). Anal. Calcd for $C_{43}H_{24}F_9IrN_{10}$: C, 49.47;H, 2.32; N, 13.42. Found: C, 49.08; H, 2.31; N, 13.10.

*mer-$[Ir(dfptrBn)_3]$ (**mer-4**).* A mixture of **1** (172 mg, 0.112 mmol), dfptrBn (64 mg, 0.235 mmol), and K_2CO_3 (155 mg, 1.12 mmol) in 2-ethoxyethanol (5 mL) was flushed with nitrogen for 20 min and refluxed for 18 h protected from light. The mixture was concentrated to dryness and extracted in dichloromethane/water. After drying the organic phase with $MgSO_4$, solvent was evaporated and the residue was purified by flash chromatography with silica gel and dichloromethane as eluent and protected from light. Yield: 60 mg (30%). ^{1}H NMR (300 MHz, $CDCl_3$): δ 7.57 (d, J = 2.1, 1H), 7.53 (d, J = 1.5, 1H), 7.50 (d, J = 1.3, 1H), 7.43−7.25 (m, 9H), 7.24−7.09 (m, 6H), 6.43 (dd, J = 8.3, 2.3, 1H), 6.34 (m, 3H), 6.12 (dd, J = 8.0, 2.2, 1H), 5.78 (dd, J = 9.5, 2.2, 1H), 5.56−5.24 (m, 6H). ^{19}F{^{1}H} NMR (282 MHz, $CDCl_3$): δ −111.38 (d, J = 7.1, 1F), −111.69 (d, J = 6.4, 1F), −112.34 (d, J = 6.0, 1F), −113.89 (d, J = 7.1, 1F), −114.01 (d, J = 6.4, 1F), −114.45 (d, J = 6.0, 1F). m/z (ESI-MS+): found 1026.210 ($[M + Na^+]^+$). Anal.

dx.doi.org/10.1021/ic3018419 | *Inorg. Chem.* 2013, 52, 1812−1824

Calcd for $C_{45}H_{30}F_6IrN_9$ C, 53.89; H, 3.01; N, 12.57. Found: C, 53.60; H, 3.30; N, 12.60

fac-[Ir(dfptrBn)$_3$] (**fac-4**). The *fac* complex was obtained by irradiation of an argon-purged MeCN solution of the *mer* complex (ca. 40 mg/3 mL) for 40 min. The product precipitates in this solvent as colorless crystals. ^{1}H NMR (300 MHz, $CDCl_3$): δ 7.53 (d, J = 2.0, 3H), 7.40−7.29 (m, 9H), 7.20−7.07 (m, 6H), 6.36 (ddd, J = 10.5, 9.3, 2.3, 3H), 6.22 (dd, J = 9.7, 2.3, 3H), 5.51−5.28 (AB system, 6H). ^{19}F{^{1}H} NMR (282 MHz, $CDCl_3$): δ −111.59 (d, J = 6.9, 3F), −114.22 (d, J = 6.9, 3F). m/z (ESI-MS+): found 1026.206 ([M + Na^+]$^+$). Anal. Calcd for $C_{45}H_{30}F_6IrN_9$ C, 53.89; H, 3.01; N, 12.57. Found: C, 53.77; H, 3.45; N, 12.66

General Procedures for Synthesis of Complexes ***mer-5***, ***mer-6***, ***fac-5***, *and* ***fac-6***. Synthesis of these complexes was adapted from already published procedures.[38] To a solution of dimer **1** in acetone (10 mL), 2 equiv of silver triflate was added and the mixture was stirred 50 °C overnight. After cooling the reaction mixture, the resulting suspension was filtered through Celite and the filtrate concentrated to dryness. Residue was dissolved in methyl ethyl ketone (MEK), and 1.5 equiv of the appropriate cyclometalating ligand and 2 equiv of triethylamine were added. The mixture was refluxed for 20 h. After cooling, the reaction mixture was concentrated to give an oily residue that was purified by flash chromatography on silica gel using hexane/EtOAc (4:1 to 2:1) as eluent to give the *mer* isomers.

The *fac* complexes were obtained by irradiation of an argon-purged MeCN solution of the respective *mer* complex (ca. 40 mg/3 mL) for 40 min. The reaction was followed by TLC and stopped when the *mer* isomer complex was consumed. Then the mixture was transferred to a flask and evaporated to dryness. Residue was suspended in dichloromethane and precipitated with MeOH. The resulting solid was filtered and washed with MeOH.

mer-[Ir(dfptrBn)$_2$(ppy)] (**mer-5**). Following the general procedure, dimer **1** (187 mg, 0.121 mmol) and silver triflate (63 mg, 0.243 mmol) were used. Chromatography has to be carried out protected from light to avoid isomerization to ***fac*-5**. Yield: 100 mg (50%). ^{1}H NMR (300 MHz, $CDCl_3$): δ 8.05 (dd, J = 5.6, 0.9 Hz, 1H), 7.90 (d, J = 8.2 Hz, 1H), 7.80−7.69 (m, 1H), 7.67−7.58 (m, 1H), 7.48 (dd, J = 5.4, 1.5 Hz, 2H), 7.38−7.29 (m, 6H), 7.21−7.09 (m, 4H), 7.09−6.93 (m, 3H), 6.94−6.80 (m, 1H), 6.42−6.27 (m, 2H), 6.09 (dd, J = 7.9, 2.2 Hz, 1H), 5.85 (dd, J = 9.5, 2.2 Hz, 1H), 5.50−5.18 (m, 4H). ^{19}F{^{1}H} NMR (282 MHz, $CDCl_3$): δ −111.40 (d, J = 6.4 Hz), −111.96 (d, J = 7.0 Hz), −113.65 (d, J = 6.4 Hz), −114.27 (d, J = 7.0 Hz). m/z (ESI-MS+): found 888.1996 ([M + H^+]$^+$), 910.1814 ([M + Na^+]$^+$). Anal. Calcd for $C_{41}H_{28}F_4IrN_7$: C, 55.52; H, 3.18, N, 11.05. Found: C, 55.20; H, 2.95; N, 10.70.

mer-[Ir(dfptrBn)$_2$(dfppy)] (**mer-6**). Following the general procedure, dimer **1** (137.5 mg, 0.089 mmol) and silver triflate (46 mg, 0.179 mmol) were used. Chromatography has to be carried out protected from light to avoid isomerization to ***fac*-6.** Yield: 114 mg (70%). ^{1}H NMR (300 MHz, $CDCl_3$): δ 8.29 (d, J = 10.9, 1H), 8.09 (dd, J = 5.6, 1.0, 1H), 7.64 (t, J = 7.8, 1H), 7.51 (m, 2H), 7.43−7.28 (m, 6H), 7.17 (td, J = 6.7, 3.0, 4H), 6.90−6.84 (m, 1H), 6.49 (dd, J = 7.9, 2.5, 1H), 6.46−6.28 (m, 3H), 6.02 (dd, J = 7.9, 2.2, 1H), 5.76 (dd, J = 9.4, 2.2, 0H), 5.36 (AB system, 4H). ^{19}F{^{1}H} NMR (282 MHz, $CDCl_3$): δ −110.60 (d, J = 8.9, 1F), −111.01 (d, J = 6.6, 1F), −111.13 (d, J = 8.9, 1F), −111.34 (d, J = 7.1, 1F), −113.37 (d, J = 6.6, 1F), −113.83 (d, J = 7.1, 1F). m/z (ESI-MS+): found 924.1833 ([M + H^+]$^+$), 946.1659 ([M + Na^+]$^+$). Anal. Calcd for $C_{41}H_{26}F_6IrN_7$: C, 53,36; H, 2,84, N, 10,62. Found: C, 53.26; H, 2,85; N, 10,35.

fac-[Ir(dfptrBn)$_2$(ppy)] (**fac-5**). After photoisomerization the compound was recrystallized in dichloromethane/Et_2O. Yield: 30 mg (from 40 mg of ***mer*-5**). ^{1}H NMR (300 MHz, $CDCl_3$): δ 7.86 (d, J = 8.2 Hz, 1H), 7.79−7.72 (m,1H), 7.71−7.56 (m, 3H), 7.51 (d, J = 2.0 Hz, 1H), 7.44−7.28 (m, 6H), 7.24−7.16 (m, 2H), 7.16−7.07 (m, 2H), 6.99−6.80 (m, 4H), 6.43−6.25 (m, 2H), 6.19 (ddd, J = 11.4, 9.8, 2.3 Hz, 2H), 5.41 (m, 4H). ^{19}F NMR (282 MHz, $CDCl_3$): δ −111.37 (d, J = 7.1 Hz), −112.13 (d, J = 6.7 Hz), −114.34 (d, J = 7.1 Hz), −114.53 (d, J = 6.7 Hz). m/z (ESI-MS+): found 888.1996 ([M + H^+]$^+$), 910.1814 ([M + Na^+]$^+$). Anal. Calcd for $C_{41}H_{28}F_4IrN_7$: C, 55.52; H, 3.18, N, 11.05. Found: C, 55.10; H, 3.01; N, 10.73.

fac-[Ir(dfptrBn)$_2$(dfppy)] (**fac-6**). Yield: 35 mg (from 40 mg of ***mer*-6**). ^{1}H NMR (300 MHz, CD_2Cl_2): δ 8.33−8.20 (m, 1H), 7.76 (dd, J = 5.6, 0.8, 1H), 7.73−7.62 (m, 3H), 7.48−7.30 (m, 6H), 7.30−7.11 (m, 4H), 6.95 (ddd, J = 7.1, 5.6, 1.2, 1H), 6.54−6.33 (m, 3H), 6.30 (dd, J = 9.3, 2.5, 1H), 6.15 (dd, J = 9.7, 2.3, 2H), 5.47 (AB system, 4H). ^{19}F{^{1}H} NMR (282 MHz, CD_2Cl_2): δ −110.25 (d, J = 9.7, 1F), −111.45 (d, J = 9.7, 1F), −111.87 (d, J = 7.1, 1F), −112.21 (d, J = 6.9, 1F), −114.05 (d, J = 7.1, 1F), −114.27 (d, J = 6.9, 1F). m/z (ESI-MS+): found 924.18 ([M + H^+]$^+$), 946.16 ([M + Na^+]$^+$). Anal. Calcd for $C_{41}H_{26}F_6IrN_7$: C, 53,36; H, 2,84; N, 10,62. Found: C, 52.76; H, 2,75; N, 10,37.

Photoisomerization. A Lot-Oriel 200 W high-pressure mercury lamp equipped with a 280−400 nm dichroic mirror (to remove IR and visible light) was used for photoisomerization of *mer* to *fac* isomers.

Photophysical Measurements. All absorption and emission spectra as well as time-resolved measurement were recorded as described elsewhere using the same equipment.[51]

X-ray Crystallography. Data set was collected with a Nonius KappaCCD diffractometer. Programs used: data collection COLLECT (Nonius B.V., 1998), data reduction Denzo-SMN,[58] absorption correction Denzo,[59] structure solution SHELXS-97,[60] structure refinement SHELXL-97,[61] graphics XP (BrukerAXS, 2000). Graphics show thermal ellipsoids with 50% probability; R values are given for the observed reflections with respect to values for all reflections.

Electrochemistry. Electrochemical characterization of the metal complexes herein reported has been performed in *N*,*N*-dimethylformamide/0.1 M tetrabutylammonium hexafluorophosphate (TBAH). Glassy carbon has been employed as working electrode, platinum wire as counter electrode, and platinum (or silver) wire as quasi-reference (QRE) electrode. For electrochemical experiments, a CHI750C Electrochemical Workstation (CH Instruments, Inc., Austin, TX) was used. Electrochemical experiments were performed in a glass cell under an argon atmosphere. To minimize the ohmic drop between the working and the reference electrodes, the feedback correction was employed. Electrochemical experiments were performed using a 1.5 mm diameter glassy carbon, GC (66-EE047 Cypress Systems), electrode. GC electrodes were stored in ethanol and before experiments polished with a 0.05 μm diamond suspension (Metadi Supreme Diamond Suspension, Buehler) and ultrasonically rinsed with ethanol for 5 min. Electrodes were electrochemically activated in the background solution by means of several voltammetric cycles at 0.5 V s^{-1} between the anodic and the cathodic solvent/electrolyte discharges until the same quality features recently described were obtained. The reference electrode was a Ag quasi-reference electrode (Ag-QRE), which was separated from the catholyte by glass frits. The reference electrode was calibrated at the end of each experiment against the ferrocene/ferricenium couple, whose formal potential is 0.464 V against the KCl saturated calomel electrode (SCE);[62] in the following, all potential values will be reported against SCE. A platinum ring or coil served as the counter electrode. In Table 4, standard potentials are calculated as the average value between cathodic and anodic peak potentials, when the processes are reversible or quasi-reversible, while the values for the HOMO−LUMO gap are calculated as the difference between the standard potential for the first oxidation and the first reduction, respectively.

Computational Methods. The ground-state geometry of the complexes has been optimized at the density functional theory (DFT) level using the Gaussian 03 package. We start from the X-ray structures, when available, and relax the geometry until atomic forces are less than 0.0001 hartree/Bohr. The chosen exchange correlation (XC) functional is the widely used B3LYP[63] in view of its good compromise between accuracy and computational cost; the basis set for description of the electrons of nonmetallic atoms is 6-31G**,[64] while the LANL2DZ basis set has been used for Ir.[65] Characterization of the nature of the lowest lying singlet and triplet excited states, involved in absorption and emission, respectively, relies on time-dependent density functional theory (TD-DFT) calculations performed on the basis of the ground-state geometry using the same functional and basis set. Figure 5 has been generated using the Jmol program [Jmol: an open-source Java viewer for chemical structures in 3D; http://www.jmol.org/. VMD: http://www.ks.uiuc.edu/Research/vmd/; Humphrey, W., Dalke, A. and Schulten, K., J. Molec. Graphics,

dx.doi.org/10.1021/ic3018419 | *Inorg. Chem.* 2013, 52, 1812−1824

Scheme 1. Schematic Procedure for the Synthesis of the Different Complexes

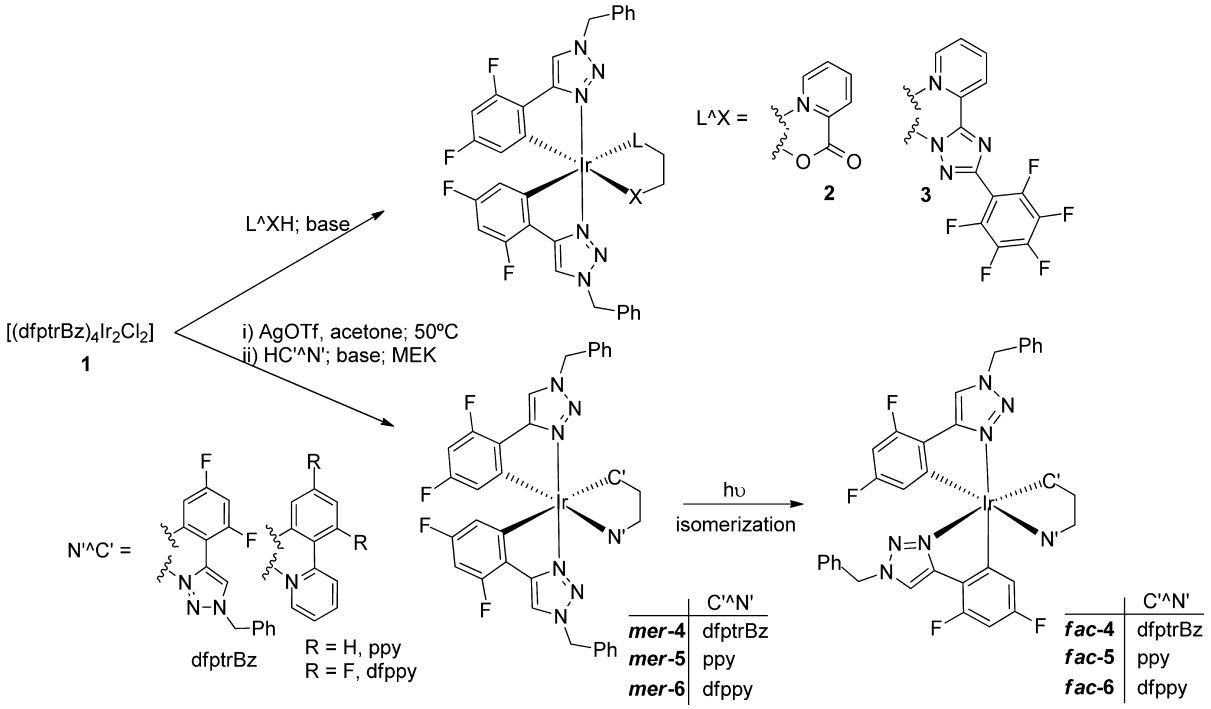

1996, 14, 33-38.] Note that the unrestricted formalism (UBLYP) has been systematically used for description of the properties related to the triplet state, while the restricted formalism has been used for those related to the singlet ground state. Our approach is motivated by previous works showing its adequacy to describe the electronic and optical properties of iridium complexes.[51,66,67] Note that these calculations neglect intersystem crossing processes mixing states of the singlet and triplet manifold.

Device Fabrication. The PLEDs were fabricated in the structure ITO/PEDOT:PSS (35 nm)/emitting layer (60−80 nm)/TPBI (30 nm)/CsF (15 Å)/Al (80 nm) in which ITO is indium tin oxide, PEDOT:PSS is poly(styrenesulfonate)-doped poly(3,4-ethylenedioxythiophene), and TPBI is 1,3,5-tris(1-phenyl-1*H*-benzimidazol-2-yl)benzene. The ITO glass substrate was treated for 10 min with UV/O_3 (UVO Cleaner 144AX, Jelight Co.) prior to any further processing. The PEDOT:PSS was spin coated directly onto ITO substrate using a spincoater P6700 from Specialty Coating Systems and then dried at 100 °C for 10 min. The emitting layer, containing a poly(*N*-vinylcarbazole) (PVK) host polymer blended with 30 wt % of 1,3-bis(5-(4-*tert*-butylphenyl)-1,3,4-oxadiazol-2-yl)benzene (OXD-7) and 7 wt % of iridium(III) complex, was spin coated on top of the PEDOT:PSS layer using chlorobenzene as the solvent; sample was then dried for 90 min at 50 °C. Prior to film casting, the polymer solution was filtered through a Teflon filter (0.45 μm). The TPBI layer was grown through thermal sublimation in a vacuum of 3×10^{-6} mbar using a MBraun evaporation chamber. The cathode was completed through thermal deposition of CsF (15 Å)/Al (80 nm). The electroluminescent device was characterized by attaching a computer-controlled low-noise single-channel direct-current (d.c.) power source that can act as both voltage source and current source and a voltage meter or current meter (Keithley 2600, Keithley Instruments). Light from the diode was coupled to a photodiode and read out by an electrometer/high-resistance meter (Keithley 6517, Keithley Instruments). The output of the data was handled by a Labview (National Instruments)-based program. Calibration of the photodiode was done at a fixed current with a luminance meter (LS-100 minolta). For every diode with a different spectral distribution of light, the photocurrent as measured by the photodiode was correlated to the light output in candelas per square meter by this calibration. The EL spectrum was obtained using a Spex FluoroLog-3 spectrofluorometer (Horiba-Jobin-Yvon Inc.).

For the OLED preparation, di-[4-(*N*,*N*-ditolyl-amino)phenyl]-cyclohexane (TAPC), 1,4-bis(triphenylsilyl)benzene (UGH2), 2,6-bis(3-(9*H*-carbazol-9-yl)phenyl)pyridine (26DCzPPy), and 1,3-bis-(3,5-dipyrid-3-yl-phenyl)benzene (BmPyPB) were purchased from Luminescence Technology Corp. and purified by sublimation before use, while Plexcore OC RG-1100 was provided by Plextronics Inc. The device structure consists of a 120 nm transparent ITO layer as the bottom electrode supported on a glass substrate. With the exception of Plexcore, which was spun on top of ITO using a Suss Microtec Delta6 RC spincoater, all other materials were vacuum deposited in an evaporation chamber at a pressure of 2.0−5.0 × 10^{-7} mbar. The ITO surface was pretreated for 10 min with UV−ozone cleaner prior to any further processing. The hole-injection layer was annealed at 180 °C for 20 min. All fabricated OLEDs were encapsulated together with an oxygen- and moisture-absorbing desiccant sheet using a glass lid and a UV-curable epoxy resin inside a nitrogen-filled glovebox. Devices were characterized optically and electrically with a C9920-12 External Quantum Efficiency Measurement System from Hamamatsu.

RESULTS AND DISCUSSION

Synthesis and Characterization. Dimer [Ir_2(dfptrBn)$_4Cl_2$] (**1**) was prepared following the procedure recently described in our group by reaction of $IrCl_3$ with the cyclometalating ligand dfptrBn in a 3:1 mixture of 2-ethoxyethanol:water at 140 °C for 20 h.[51,52] We have shown the utility of **1** as precursor for preparation of cationic bis-cyclometalated Ir(III) complexes.[51] Furthermore, this dimer can also be used as starting material for synthesis of neutral bis-cyclometalated and tris-cyclometalated Ir(III) complexes (Scheme 1). By refluxing a suspension of **1** in a dichloromethane:ethanol mixture (3:1) with picolinic acid (picH) or 2-(5-(perfluorophenyl)-2*H*-1,2,4-triazol-3-yl)pyridine (pytrF_5) in the presence of a base, neutral complexes, [Ir(dfptrBn)$_2$(pic)] (**2**) and [Ir(dfptrBn)$_2$(pytrF_5)] (**3**), were obtained in high yields (Scheme 1). On the other hand, the facial (*fac*) tris-cyclometalated homoleptic complex, *fac*-[Ir(dfptrBn)$_3$] (***fac*-4**), and heteroleptic complexes, *fac*-[Ir(dfptrBn)$_2$(ppy)] (***fac*-5**) and *fac*-[Ir(dfptrBn)$_2$(dfppy)] (***fac*-6**), were synthesized modifying

dx.doi.org/10.1021/ic3018419 | *Inorg. Chem.* 2013, 52, 1812−1824

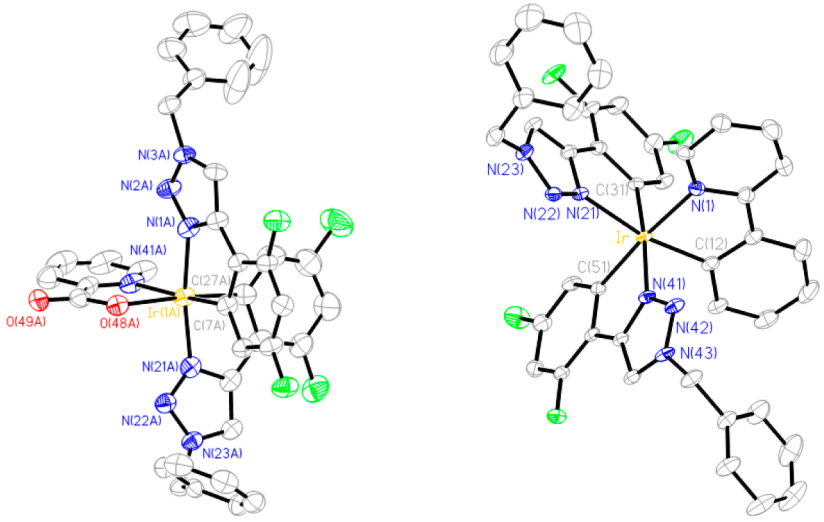

Figure 1. Crystal structure of **2** (left) and ***fac*-5** (right). Selected parameters of the crystal structures are shown in Tables S1 and S2, Supporting Information.

a procedure described in the literature (Scheme 1).[38] First, the meridional (*mer*) isomers, ***mer*-4**, ***mer*-5**, and ***mer*-6**, were isolated by reaction of **1** and AgOTf in acetone followed by addition of the corresponding cyclometalating ligand and a base (Scheme 1). Subsequently, the meridional isomers were transformed to their facial counterparts by irradiation of degassed MeCN solutions of the corresponding complexes with UV light (Scheme 1). All complexes were characterized using ^{1}H NMR, ^{19}F NMR, high-resolution mass spectrometry, and elemental analysis (see Experimental Section).

For complexes **2** and ***fac*-5**, single crystals suitable for X-ray crystallographic analysis were obtained by crystallization in acetonitrile/Et_2O and chloroform/Et_2O, respectively (Figure 1).

In both complexes, the central Ir atom is in a distorted octahedral coordination geometry. For complex **2**, two independent molecules (molecules A and B) are observed in the unit cell (probably due to packing effects) and the distances are equal within three standard deviations for both molecules (Figure S1, Supporting Information). It is interesting to compare the crystal structure of **2** and the structure of the analogous complex with dfppy as cyclometalated ligand, the well-known [Ir(dfppy)$_2$(pic)] (FIrpic) that was described elsewhere.[68] In FIrpic, both Ir−C distances are very similar (1.994(4) and 1.997(5) Å) and shorter than in **2** (2.032(11) and 2.068(8) Å for molecule A, 2.028(8) and 2.059(8) Å for molecule B), while the Ir−$N_{pyridine}$ of cyclometalated dfppy (2.041(4) and 2.045(4) Å) is slightly longer compared to Ir−$N_{triazole}$ in **2** (2.029(7) and 2.037(8) Å for molecule A, 2.019(7) and 2.036(7) Å for molecule B). Ir−O distances in **2** are 2.162(7) Å for molecule A and 2.163(5) Å for molecule B and similar to the distance found in FIrpic (2.152(3) Å). There is no indication for $\pi-\pi$ interactions since the shortest distance between the centers of the benzyl groups is 5.093 Å.

The crystal structure of complex ***fac*-5** confirms the facial arrangement of the cyclometalated ligands in the complex. The three Ir−C distances in ***fac*-5** are similar (Ir−C(12) = 2.021(5) Å, Ir−C(31) = 2.045(5) Å, and Ir−C(51) = 2.037(4) Å), also when compared to Ir−C (2.016 Å) found in the homoleptic complex *fac*-[Ir(ppy)$_3$].[69] On the other hand, Ir−N(21) (2.153(4) Å) is slightly longer than the other two Ir−N distances in the complex (Ir−N(1) = 2.123(4) Å and Ir−N(41) = 2.121(4) Å), probably due to packing effects. We find no indication of $\pi-\pi$ interactions since the shortest distance between the centers of the benzyl groups is 6.141 Å.

Quantum-Chemical Calculations. Optimized geometrical parameters calculated for complexes **2** and ***fac*-5** are in good agreement with X-ray experimental data (Table S3, Supporting Information); this ensures a proper description of the nature of the lowest excited states, provided that the complex keeps a similar geometry in solution. In a second step, we examined the nature of the frontier electronic levels that will be predominantly involved in the lowest excited states of all complexes by analyzing for each electronic level the contribution from the different fragments (Table 1).

Table 1 shows that the HOMO orbital is mainly localized on the iridium atom (around 50%) for all complexes, except complex **3** for which the major contribution of the HOMO orbital (61%) lies on the coordinating ligand (pytrF$_5$), with only 23% on the iridium atom. Among the six highest occupied molecular orbitals, all complexes exhibit three molecular orbitals with a large contribution from the iridium atom (HOMO, HOMO-1, and HOMO-5 for complexes **2** and **3** and HOMO, HOMO-1, and HOMO-2 for complexes ***fac*-4**, ***fac*-5**, and ***fac*-6**). For the three other orbitals, a significant contribution can be observed from different ligands. While most of the complexes have their HOMO level in the same energy range (from −5.25 to −5.00 eV), complex **3** has a much deeper HOMO level (−5.49 eV). All complexes exhibit the same pattern for localization of the LUMO orbital; in all cases, the contribution from the coordinating ligand exceeds 90% (see also Figure 2). None of the six lowest unoccupied orbitals has a large contribution from the iridium atom. Note that each ligand has at least one significant contribution in one of the LUMO levels listed in Table 1. In contrast to the HOMO level, the energies of the LUMO level vary much more among the complexes (−0.63, −1.10, −1.18, −1.29, and −1.45 eV for complexes ***fac*-4**, ***fac*-5**, ***fac*-6**, **2**, and **3**, respectively).

Photophysical properties and DFT Calculations. It is well known that *mer* isomers have different spectroscopic properties compared to *fac* geometries, with lower quantum yields and poor photostability that make them not suitable for photonic applications.[37,38] In our systems we faced the same problems with the stability of the *mer* isomers compared to the

dx.doi.org/10.1021/ic3018419 | *Inorg. Chem.* 2013, 52, 1812−1824

Table 1. Energy (in eV) and Localization of the Frontier Electronic Levels from HOMO-5 to LUMO+5 in Complexes 2, 3, *fac*-4, *fac*-5, and *fac*-6[a]

complex **2**					
				dfptrBn	
FO	eV	Ir	pic	transN	transO
HOMO-5	−6.27	54	8	14	24
HOMO-4	−6.01	21	4	15	60
HOMO-3	−5.94	7	41	42	11
HOMO-2	−5.86	2	64	23	10
HOMO-1	−5.64	46	31	16	8
HOMO	**−5.25**	**48**	**9**	**23**	**20**
LUMO	**−1.29**	**3**	**95**	**1**	**1**
LUMO+1	−0.91	3	14	14	69
LUMO+2	−0.87	4	4	73	19
LUMO+3	−0.76	3	61	15	22
LUMO+4	−0.64	2	8	30	60
LUMO+5	−0.61	1	6	80	12

complex **3**					
				dfptrBn	
FO	eV	Ir	pytrF5	transN	trans3N
HOMO-5	−6.38	45	31	12	12
HOMO-4	−6.28	0	98	1	0
HOMO-3	−6.18	14	2	19	66
HOMO-2	−5.99	9	4	72	14
HOMO-1	−5.57	35	22	15	27
HOMO	**−5.49**	**23**	**61**	**5**	**11**
LUMO	**−1.45**	**4**	**93**	**1**	**2**
LUMO+1	−1.10	5	7	8	80
LUMO+2	−0.95	4	41	39	16
LUMO+3	−0.89	4	18	45	34
LUMO+4	−0.80	2	29	15	53
LUMO+5	−0.60	1	1	3	96

complex ***fac*-4**					
FO	eV	Ir	dfptrBn1	dfptrBn2	dfptrBn3
HOMO-5	−5.83	10	33	31	26
HOMO-4	−5.71	9	50	35	5
HOMO-3	−5.71	9	7	24	60
HOMO-2	−5.29	45	25	24	6
HOMO-1	−5.28	45	12	14	30
HOMO	**−5.13**	**49**	**17**	**16**	**18**

complex ***fac*-4**					
FO	eV	Ir	dfptrBn1	dfptrBn2	dfptrBn3
LUMO	**−0.63**	**2**	**90**	**6**	**2**
LUMO+1	−0.62	2	6	89	3
LUMO+2	−0.60	2	2	2	93
LUMO+3	−0.44	1	51	35	13
LUMO+4	−0.41	1	42	56	1
LUMO+5	−0.40	1	6	8	85

complex ***fac*-5**					
				dfptrBn	
FO	eV	Ir	ppy	transN	transC
HOMO-5	−5.91	5	81	5	8
HOMO-4	−5.74	7	10	24	59
HOMO-3	−5.66	7	2	64	27
HOMO-2	−5.19	48	6	17	29
HOMO-1	−5.14	49	17	22	12
HOMO	**−5.00**	**51**	**28**	**12**	**9**
LUMO	**−1.10**	**4**	**93**	**2**	**1**
LUMO+1	−0.80	2	4	2	92
LUMO+2	−0.66	3	79	7	11
LUMO+3	−0.60	3	4	90	3
LUMO+4	−0.55	1	5	1	94
LUMO+5	−0.40	1	1	97	1

complex ***fac*-6**					
				dfptrBn	
FO	eV	Ir	dfppy	transN	transC
HOMO-5	−5.94	7	59	12	22
HOMO-4	−5.82	6	33	15	46
HOMO-3	−5.77	8	3	64	25
HOMO-2	−5.36	48	28	8	16
HOMO-1	−5.33	46	7	28	18
HOMO	**−5.20**	**51**	**14**	**18**	**16**
LUMO	**−1.18**	**4**	**92**	**2**	**1**
LUMO+1	−0.87	2	3	2	93
LUMO+2	−0.69	2	26	63	9
LUMO+3	−0.66	3	37	36	24
LUMO+4	−0.61	1	18	3	78
LUMO+5	−0.46	1	1	97	1

[a]We defined the following fragments: Ir, ligands (pic, pytrF5, ppy, and dfppy), and cyclometalated dfptrBn which are characterized with respect to the bond in trans of the atom in the coordinating ligand (pic, pytrF5, ppy, and dfppy for complexes **2**, **3**, ***fac*-5**, and ***fac*-6**, respectively).

fac analogues (see Table S5 in Supporting Information), and therefore, we focused only on the photophysical properties of the *fac* isomers, while the photophysics for the *mer* isomers are reported in the Supporting Information.

Absorption spectra of complexes **2**, **3**, ***fac*-4**, ***fac*-5**, and ***fac*-6** were recorded at room temperature in dichloromethane solutions (Figure 3), and absorbance values of the most important bands are shown in Table 2.

The intense bands ($\varepsilon > 10^4$ cm^{-1} M^{-1}) in the region 230−320 nm are assigned to $\pi-\pi^*$ transitions localized on the coordinated ligands, while the bands at lower energy are typically assigned to spin-allowed and spin-forbidden ligand-centered (LC) and metal-to-ligand charge transfer (MLCT) transitions.

In complexes **2** and **3**, the absorbance bands at low energy (>320 nm) are blue shifted compared to the dfppy counterparts.[54,55] For the homoleptic complex ***fac*-4**, the MLCT transitions are higher in energy than for the dfppy analogue, [Ir(dfppy)$_3$].[37] This is due to an increase in the energy gap between the metal d orbitals and the π^* orbitals of the cyclometalating ligand, because of the higher energy of π^* orbitals observed for triazole compared to pyridine moieties.[49,70] This is also observed for phenylpyrazolyl-based Ir(III) complexes.[37,38] Furthermore, complexes ***fac*-5** and ***fac*-6** have in general a higher extinction coefficient compared to **2**, **3**, or ***fac*-4** due to the presence of arylpyridine ligand. For complexes **3**, ***fac*-4**, ***fac*-5**, and ***fac*-6**, the weak absorption band at 420, 392, 467, and 450 nm, respectively, could be assigned to a spin-forbidden singlet-to-triplet transition. These transitions might be partially allowed due to the presence of a heavy atom, such as iridium, with a strong spin−orbit coupling. Indeed, these values are similar to the one observed for the first band in the emission spectra at low temperature for these complexes (Table 2).

We further calculated the nature of the lowest singlet excited states at the TD-DFT level to assist interpretation of the experimental spectra. Figure S2 and Table S4 (Supporting

dx.doi.org/10.1021/ic3018419 | Inorg. Chem. 2013, 52, 1812−1824

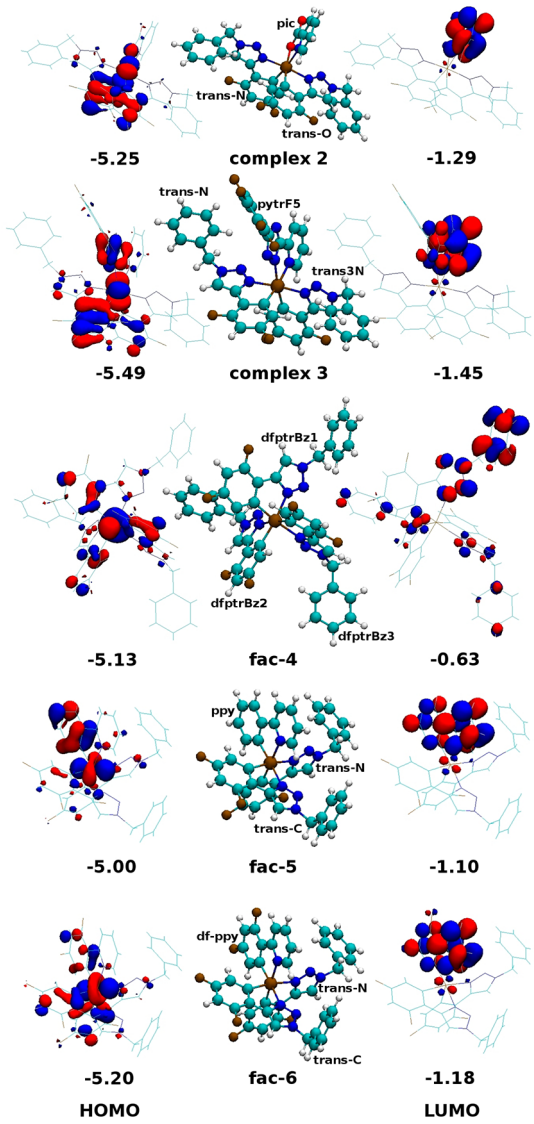

Figure 2. Representation of the optimized molecular geometry of the complexes and of the localization of the HOMO (left) and LUMO (right) orbitals. Labels of the different ligands used in Table 1 are also displayed.

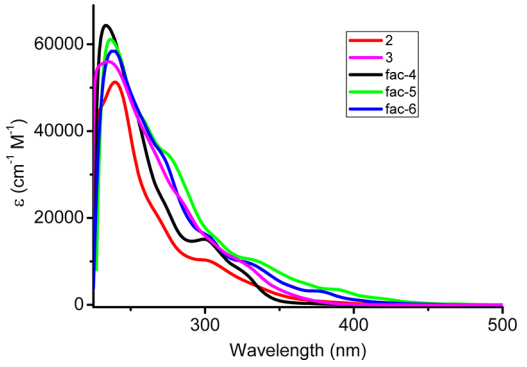

Figure 3. Absorbance spectra in aerated dichloromethane solutions of complexes **2**, **3**, ***fac*-4**, ***fac*-5**, and ***fac*-6**.

Information) summarize the experimental absorption features of the complexes in dichloromethane as well as the excited states (ES) contributing to the absorption peaks according to the TD-DFT calculations. Theoretical results for complexes **2** and **3** match well the experimental results. The energies of the different absorption bands are well reproduced. For complex **2**, the absorption peaks at low energy have mainly MLCT and ligand-to-ligand charge transfer (LLCT) character. The calculated absorption peak at 383 nm (ES1, Table S4, Supporting Information) involves the LUMO orbital which is localized on the pic ligand; the MLCT thus occurs between the iridium atom and the pic ligand, while the LLCT occurs between the transN dfptrBn and transO dfptrBn ligands and the pic ligand. For all absorption bands listed in Table S4, Supporting Information, the MLCT always occurs from the iridium atom to the pic (383 (ES1) and 342 nm (ES3)) or transO dfptrBn (345 nm (ES2)) ligands, while transfers to the transN dfptrBn ligand are negligible. At higher energy, the intensity of the peaks grows as a result of introduction of an increasing ligand-centered (LC) character. The first LC contribution arises from the ligand transO dfptrBn (ES55), then from transN dfptrBn (ES57), and finally from pic (ES82). For complex **3**, surprisingly, the first absorption peak has mainly LC character, in addition to a MCLT character. That the MLCT character is not the dominant character for this peak results from the much lower localization of the HOMO orbital on the iridium atom (only 23%) compared to complex **2**. Since the HOMO and LUMO levels are mainly localized on the coordinating ligand ($pytrF_5$), it has a dominant intraligand charge transfer character. Moreover, the weak intensity of the absorption band can be easily understood since the HOMO and LUMO levels lay on different parts of the $pytrF_5$ ligand. At higher energy, the contribution of the aryltriazole ligand increases the LLCT character of the absorbance, although the LC character involving the $pytrF_5$ ligand is still important. For the facial complexes, the simulations systematically overestimate the energy of the lowest two absorption peaks (by about 0.5 eV, because the solvent effects have been neglected and/or the uncertainty in the experimental value due to possible spin-forbidden transitions of low intensity), while good agreement is obtained at higher energy. However, the relative shifts between the energy of the various absorption bands of ***fac*-4**, ***fac*-5**, and ***fac*-6** are well reproduced. Given that ***fac*-4** is a homoleptic complex, the number of transitions contributing to an absorption band is much larger compared to all other complexes since all ligands are identical in ***fac*-4**. In fact, the lowest simulated absorption band is made of three dominant excited states involving an electron transition from the HOMO level to the LUMO, LUMO+1, and LUMO+2 level. All these transitions can be considered as equivalent since the quasi-degenerate LUMO, LUMO+1, and LUMO+2 are localized on the three different ligands (vide supra). Complexes ***fac*-5** and ***fac*-6** are only differing by the presence of two fluorine atoms on the ppy ligand in ***fac*-6**. Therefore, the energy as well as the nature of the transitions in the absorption bands are quite similar. In both cases, the lowest three absorption bands have a strong MLCT character involving a transition from the iridium atom to the ppy (dfppy) ligand for ***fac*-5** (***fac*-6**). The fourth absorption band is characterized in both complexes by MLCT character from the iridium atom to the three ligands. At higher energy, a LC contribution is relevant to the excited states. For the fifth absorption band, the LC character involves the ppy (ES27,ES28) for **fac-5** and dfppy (ES20,ES22) for ***fac*-6**, while for the next absorption band, it is mainly the transC dfptrBn ligand even though transN dfptrBn has a small contribution. Note also that in Figure S2, Supporting Information, the

dx.doi.org/10.1021/ic3018419 | *Inorg. Chem.* 2013, 52, 1812−1824

Table 2. Photophysical Data of Iridium Complexes

complex		abs, λ/nm (ε, $M^{-1}cm^{-1}$)	em, λ/nm	Φ^c	τ (μs)	k_r (10^5 s^{-1})	k_{nr} (10^5 s^{-1})
2	solution[a]	240(49 000) 268(sh)(20 000) 300 (10 000) 395 (750)	498	0.012[d] (0.009)[e]	0.027[d] (0.021)[e]	4.4	365.8
	butyronitrile glass[b]		458		12.6		
3	solution	234 (59 900) 284(25 200) 323(10 000) 420(35)	440, 462	0.05[d] (0.01)[e]	0.56[d] (0.16)[e]	0.9	16.9
	butyronitrile glass[b]		425, 454, 480		5.6		
***fac*-4**	solution[a]	234(64 216) 257(sh)(41 330) 300 (15 093) 323(8240) 371(224) 392(72)					
	butyronitrile glass[b]		392, 418		13.8		
***fac*-5**	solution[a]	236(61 100) 257(43 700) 274(21 593) 332(9400) 387(2450) 417(1574) 467(136)	480, 510	0.76[d] (0.04)[e]	2.6[d] (0.09)[e]	2.9	0.9
	neat film		487, 513	0.18	0.32(29%) 0.77(71%)		
	10% PMMA		480, 510	0.50	1.73(17%) 3.06(83%)		
	butyronitrile glass[b]		467, 492, 501, 528		4.43		
***fac*-6**	solution[a]	241 (58 625) 270 (34 857) 301(16 338) 325 (9956) 377(1033) 422(368) 450(143)	465, 489	0.50[d] (0.06)[e]	1.15[d] (0.1)[e]	4.3	4.3
	neat film		467, 490	0.15	0.27(41%) 0.60(59%)		
	10% PMMA		461, 488	0.42	0.90(15%) 2.29(85%)		
	butyronitrile glass[b]		448, 472, 480, 509		3.60		

[a]Solution in dichloromethane. [b]At 77K. [c]PL QYs were determined with a calibrated integrating sphere system. [d]Deaerated solution. [e]Aerated solution.

relative intensities of the absorption bands are well reproduced for the five complexes.

Experimentally, complex **2** presents an unstructured emission spectrum with a maximum at 498 nm in dichloromethane solution at room temperature (Figure 4). This emission maximum is blue shifted (1105 cm^{-1}, 30 nm) compared to the analogous 1,4-disubstituted-1*H*-1,2,3-triazole complex, [Ir(C^N)$_2$(pic)] (C^N = 1-decyl-4-phenyl-1*H*-[1,2,3]triazolyl), (λ_{em} = 527 nm) described recently in the literature[49] due to the presence of fluorine atoms in our compound. However, the emission is red shifted compared to the arylpyridine counterparts, FIrpic (λ_{em} = 468 nm).[54,56] Furthermore, the 77 K spectrum in butyronitrile glass has a maximum at 458 nm and is blue shifted compared to the emission in solution. Interestingly, it still shows a broad emission that would correspond to a high MLCT character of the excited state, which agrees with theoretical results (see below). To gain insight into the CT character of the excited state, emission spectra of complex **2** in different solvents at room temperature have been further studied (Figure S3, Supporting Information). Thus, by increasing the polarity of the solvent, e.g., toluene, dichloromethane, MeCN and formamide the emission maxima shift to the red, λ_{em} = 475, 498, 508, and 534 nm, respectively. This strong solvatochromic behavior is in agreement with a pronounced CT character of the excited state, as confirmed by calculations (see below). The excited-state lifetimes are short, both in the presence and in the absence of oxygen, τ_{aer} = 21 ns and τ_{deaer} = 27 ns, respectively. Furthermore, the emission quantum yields (QY) mirror this behavior being around 0.9% and 1.2% in aerated and deaerated solutions, respectively.

Complex **3** has a structured emission spectrum at room temperature with maxima at 440 and 462 nm, while at 77 K the

dx.doi.org/10.1021/ic3018419 | Inorg. Chem. 2013, 52, 1812−1824

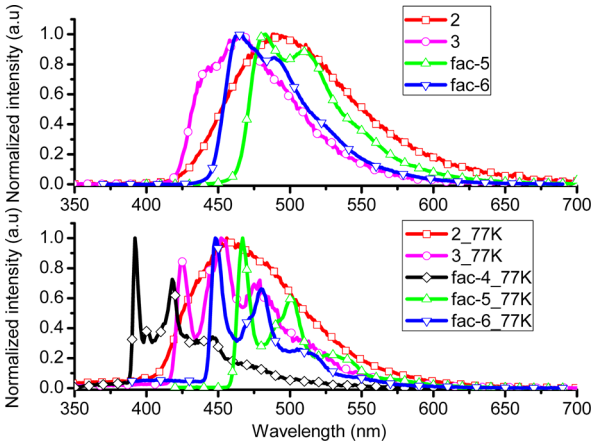

Figure 4. Emission spectra of the investigated complexes in dichloromethane at RT (top) and butyronitrile glass matrix at 77 K (bottom).

spectrum is slightly blue shifted and much more structured (Figure 4). The emission in solution is ca. 20 nm (890 cm^{-1}) blue shifted compared to the one observed for the dfppy analogue, $[Ir(dfppy)_2(pytrF_5)]$, synthesized in our group.[55] Furthermore, complex **3** shows a QY of 5% and a short excited-state lifetime (0.56 μs) in deaerated solutions that yields a high nonradiative rate constant (k_{nr}). The high value for k_{nr} could be related to a distortion from coplanarity between the triazole of the $pytrF_5$ ligand and the substituted pentafluorophenyl ring connected to it, as observed in complex $[Ir(dfppy)_2(pytrF_5)]$,[55,71] although the QY (16%) is higher in the latter. In fact, the DFT results show that the excited state is more localized on the dfppy ligand for $[Ir(dfppy)_2(pytrF_5)]$,[71] while in **3** it is more localized on the $pytrF_5$ (see below).

On the other hand, homoleptic ***fac*-4** shows no emission in solution at RT but a structured deep-blue emission at 77 K in butyronitrile glass matrix (Figure 4). This behavior is similar to the one found for the analogous complex with difluorophenylpyrazole (dfppz) as the cyclometalating ligand, $[Ir(dfppz)_3]$.[36−38] However, the lifetime for ***fac*-4** (13.2 μs) is almost one-half that of the corresponding dfppz (27 μs). Accordingly, we assign the excited state to a mixed MLCT/LC character. We believe that the reasons for the lack of luminescence at room temperature of complex ***fac*-4** are the same as for *fac*-$[Ir(dfppz)_3]$, i.e, a thermal activation of a nonradiative state, formed by decoordination of the N-heterocyclic ring in the excited state.[36,72] A similar explanation was used by Samuel et al. to justify the lowering in the emission in a series of phenyl-1,2,4-triazoles Ir(III) complexes.[45]

Complexes ***fac*-5** and ***fac*-6** present structured emission spectra in solution at room temperature, while emission spectra in butyronitrile glass matrix at 77 K show a much more structured and blue shifted emission (Figure 4). This behavior supports the MLCT character of the lowest-lying excited state with a pronounced LC character, similar to what was observed for the phenylpyrazolyl analogues.[38] Both complexes show a high QY in deaerated solution. The lifetimes of the excited state of complexes ***fac*-5** and ***fac*-6** in deaerated solutions are 2.6 and 1.15 μs, respectively, while in air-equilibrated solutions they are shorter and in the range of 0.1 μs. This is in accordance with the triplet character of the lowest lying excited states, a mixed ^{3}LC/^{3}MLCT. In both cases, lifetime decays were mono-exponential. Interestingly, emission of ***fac*-6** (λ_{em} = 465 nm) is blue shifted compared to ***fac*-5** (λ_{em} = 480 nm) when changing from ppy to dfppy due to the presence of fluorine atoms that lower the HOMO. Additionally, the presence of aryltriazole as cyclometalating ligand in ***fac*-5** and ***fac*-6** shifts the emission maxima to the blue compared to homoleptic complexes *fac*-$[Ir(ppy)_3]$ (λ_{em} = 509 nm) and *fac*-$[Ir(dfppy)_3]$ (λ_{em} = 469 nm) described in the literature.[36,37] The photophysical properties in solution of complexes ***fac*-5** and ***fac*-6** make them promising candidates as dopants in electroluminescent devices (see below). Thus, the emission properties in thin films, both neat films and 10 wt % doped in a poly(methyl methacrylate) (PMMA) films, were studied. For both complexes, the emission spectra in neat film are slightly red shifted compared to solution or 10 wt % doped film spectra while the latter are almost identical to the spectra in solution (Table 2 and Figure S4, Supporting Information). The QYs in neat films (18% for ***fac*-5** and 15% for ***fac*-6**) are significantly lower than the QY in doped films (50% for ***fac*-5** and 42% for ***fac*-6**). Furthermore, the lifetimes in neat film are significantly shorter than the ones observed in 10 wt % doped films (Table 2). The higher quenching observed in neat films compared to the diluted films is due to a higher degree of triplet−triplet annihilation. It is interesting to compare the emission of complexes ***fac*-5** and ***fac*-6** with their phenylpyrazolyl counterpart described in the literature.[36−38] Thus, complexes ***fac*-5** and ***fac*-6** mimic the behavior of the dfppz analogues, *fac*-$[Ir(dfppz)_2(ppy)]$ (λ_{em} = 475 nm, QY = 0.93, τ = 2.6 μs)[36] and *fac*-$[Ir(dfppz)_2(dfppy)]$ (λ_{em} = 457 nm, QY = 0.60, τ = 1.3 μs).[36] The higher QY of ***fac*-5** could be due to higher activation energy of the nonradiative state compared to ***fac*-6**.[36]

Table 3 summarizes the TD-DFT-calculated nature of the lowest triplet excited state for all complexes. It shows a nice agreement with the experimental results except for complex **2** for which the calculated emission band is blue shifted by *ca.* 100 nm while it is only about 30 nm for the other complexes. Among the facial isomers, the emission band at higher energy of ***fac*-4** is well reproduced as well as the impact of the fluorination of ppy on ***fac*-6**. A graphical representation of the character of the triplet state is displayed in Figure 5. For complexes **3**, ***fac*-5**, and ***fac*-6**, Figure 5 demonstrates that the triplet state has a strong intraligand charge-transfer character and a small MLCT character. In contrast, for ***fac*-4**, all fragments of the complex are involved. For complex **2**, the triplet excited state has mainly MLCT and LLCT characters. The large discrepancy observed in the calculations and experimental data for **2** might be partly rationalized by the large observed solvatochromism due to the strong CT character

Table 3. Characterization of the Lowest Triplet Excited State at the TD-DFT Level in the Absence of Spin−Orbit Coupling for Complexes 2, 3, *fac*-4, *fac*-5, and *fac*-6

complex	occ	vir	eV/nm	%
2	HOMO	LUMO	3.16/392	50
	HOMO-2	LUMO		27
3	HOMO-1	LUMO	2.90/428	49
	HOMO	LUMO		40
***fac*-4**	HOMO	LUMO+10	3.34/371	16
	HOMO-1	LUMO+11		11
***fac*-5**	HOMO	LUMO	2.75/450	41
	HOMO-5	LUMO		19
***fac*-6**	HOMO	LUMO	2.88/430	29
	HOMO-5	LUMO		17

dx.doi.org/10.1021/ic3018419 | *Inorg. Chem.* 2013, 52, 1812−1824

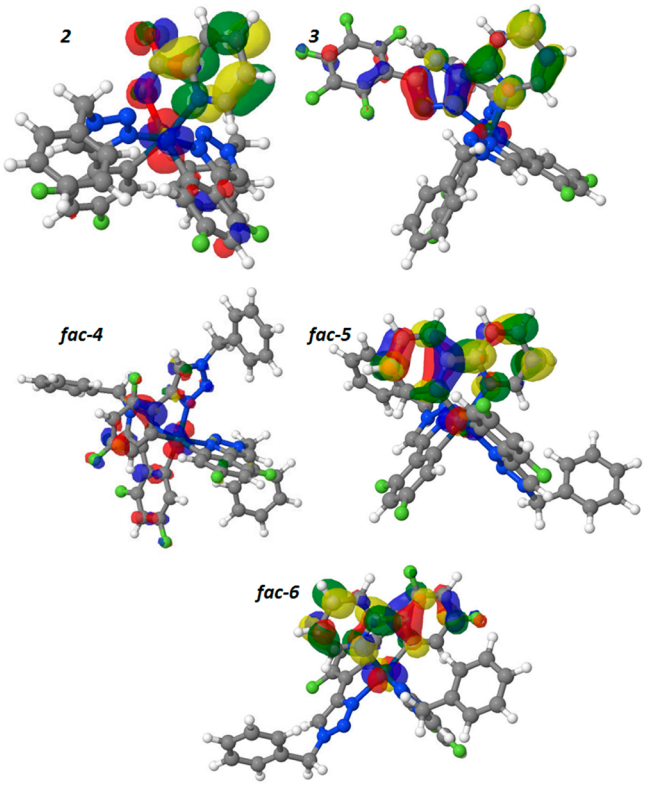

Figure 5. Representation of the character of the triplet state. Red/blue [yellow/green] isosurface is generated by the Jmol program [Jmol: an open-source Java viewer for chemical structures in 3D; http://www.jmol.org/. VMD: http://www.ks.uiuc.edu/Research/vmd/; Humphrey, W., Dalke, A. and Schulten, K., J. Molec. Graphics, 1996, 14, 33-38.] by combining for each atom the LCAO coefficients in all occupied [unoccupied] molecular orbitals involved in the TD-DFT description of the triplet state and their CI contributions.

of the excited state (see above). To complement our description of the T1 state, a spin density analysis has been performed. Figure S5, Supporting Information, confirms the TD-DFT analysis. The spin densities are localized in the iridium atom and one ligand for complexes **3**, ***fac*-5**, and ***fac*-6** while for **2** and ***fac*-4**, they are more distributed over the whole complex.

Electrochemistry. The cyclic voltammetry (CV) of complexes ***fac*-5** and ***fac*-6** was measured in 0.1 M solution of TBAH in DMF, and the potentials referenced to SCE (Table 4).

Table 4. Electrochemical Data of Iridium Complexes[a]

complex	E_{ox} (V)	E_{red} (V)	E_{HOMO} (eV)	E_{LUMO} (eV)	$\Delta E_{HOMO-LUMO}$ (eV)
***fac*-5**	+1.06[b,d]	−2.27[e]	−5.86[f]	−2.53[f]	3.33[g]
***fac*-6**	+1.24[c,d]	−2.17[e]	−6.04[f]	−2.63[f]	3.41[g]

[a]Cyclic voltammetry recorded in DMF/0.1 M TBAH. [b]Quasi-reversible process (ΔE_p > 60 mV).[73] [c]Reversible process ($\Delta E_p \approx$ 60 mV). [d]E_{ox} has been evaluated as the mean value between the anodic and cathodic peak potential. [e]Irreversible process: E_{red} is related to the cathodic peak potential. [f]Energy levels (HOMO and LUMO) are calculated referring to the energy level of ferrocene/ferricenium couple.[74] [g]HOMO−LUMO energy gap, measured by cyclic voltammetry and calculated upon conversion of mV to eV.[74]

In both cases, they show an irreversible reduction at all scan rates (up to 5 V s^{-1}), while the oxidation is reversible for ***fac*-6** and quasi-reversible for ***fac*-5** since the peak-to-peak separation (ΔEp) is greater than 80 mV even for slower scan rate. In all the cases, the ratio between cathodic and anodic peak currents is ∼1. In good agreement with the DFT calculations, the oxidation for complex ***fac*-5** is associated with the phenyl of the ppy and the Ir atom, while for ***fac*-6** it is located on the difluorophenyl moieties and the iridium atom. Additionally, the reduction occurs on the pyridine of the ppy ligand for ***fac*-5** and on the pyridine of the dfppy for ***fac*-6**, according to the DFT calculations. Interestingly, the reduction potential for ***fac*-6** is 100 mV higher (0.080 eV energy difference at the DFT level) than for ***fac*-5** due to the electron-withdrawing effect of the fluorine atoms in the dfppy unit, resulting in a higher LUMO for ***fac*-5**. Furthermore, fluorine substituents on dfppy also affect the oxidation potential of ***fac*-6**, which is observed to be 200 mV (0.2 eV also at the DFT level) higher than for ***fac*-5**. Taking into account these results, we can therefore conclude that the fluorination of the ppy ligand in these complexes lowers the LUMO in a lesser extent than the HOMO, giving rise to an increase in the HOMO−LUMO gap in ***fac*-6** compared to ***fac*-5** as observed by the ΔE 70 meV higher for the former. This effect is similar to the one observed for the phenylpyrazole analogues.[38]

Electroluminescent Devices. Due to their high luminescence quantum yields in solution and thin films, complexes ***fac*-5** and ***fac*-6** were selected as triplet emitter in the fabrication of polymer light-emitting diodes (PLEDs). Furthermore, emitter ***fac*-6** was selected for further tests as dopant in small-molecule OLEDs prepared by vacuum deposition because of its more saturated blue color.

For the PLEDs, we used a host matrix containing poly(*N*-vinylcarbazole) (PVK) and 1,3-bis(5-(4-*tert*-butylphenyl)-1,3,4-oxadiazol-2-yl)benzene (OXD-7) for achieving optimal environment for these blue phosphorescent complexes. The device configuration consists of ITO/PEDOT:PSS (35 nm)/PVK:OXD-7 (30 wt %):Ir complex (7 wt %) (60−80 nm)/TPBI (30 nm)/CsF (15 Å)/Al (80 nm), in which ITO, PEDOT:PSS, and TPBI stand for indium tin oxide, poly(styrenesulfonate)-doped poly(3,4-ethylenedioxythiophene), and 1,3,5-tris(1-phenyl-1*H*-benzimidazol-2-yl)benzene, respectively.

The EL spectrum and representative performance data of Ir(III) complexes are depicted in Figure 6 and Table 5,

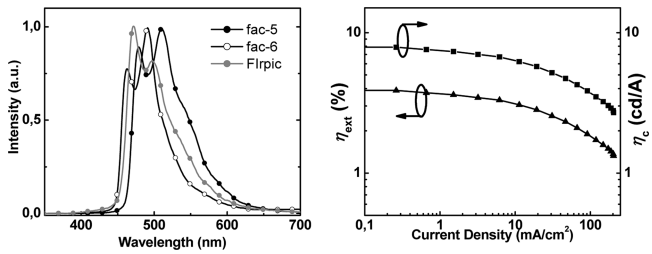

Figure 6. (a) EL spectra (at around 100 cd/m^2) of the studied PLED devices doped with ***fac*-5** and ***fac*-6** and FIrpic. (b) External quantum efficiency (η_{ext}) and luminous efficiency (η_c) vs current density for the ***fac*-6**-based diode with device configuration ITO/PEDOT:PSS/PVK:OXD-7:7 wt % ***fac*-6**/TPBI/CsF/Al.

respectively. The EL spectrum shows a dominant emission from the Ir(III) complex without any other residual emission from host and/or adjacent layers, thus revealing effective energy transfer from the host to Ir dopants. The 1931 Commission Internationale de L'Eclairage coordinates (CIE) of ***fac*-5** and

dx.doi.org/10.1021/ic3018419 | *Inorg. Chem.* 2013, 52, 1812−1824

Table 5. Summary of PLED Characteristics Using *fac*-5, *fac*-6, and FIrpic as Dopants

	V_{on}[a] [V]	L_{max} [cd/m^2]	$\eta_{ext,max}$[b] [%]	$\eta_{c,max}$[b] [cd/A]	fwhm [nm]	$CIE_{x,y}$[c]
***fac*-6**	3.4	5587	3.9	8.0	55	(0.17, 0.34)
***fac*-5**	3.4	21 285	6.0	16.4	78	(0.22, 0.52)
FIrpic	3.7	7792	3.8	8.5	60	(0.19, 0.40)

[a]Recorded at 1 cd/m^2. [b]External quantum efficiency: η_{ext}. Luminous efficiency: η_c. [c]At around 100 cd/m^2.

***fac*-6** calculated from the EL spectrum at around 100 cd/m^2 are (0.22, 0.52) and (0.17, 0.36), respectively. Upon varying the driving voltage from 5 to 13 V, the EL spectra barely change (Figure S6, Supporting Information) and the CIE values remain almost constant. Among these two Ir emitters, the CIE coordinates of the device incorporating ***fac*-6** indicate purer and bluer emission than the device doped with FIrpic. The ***fac*-6**-based device exhibits a turn-on voltage at 3.4 V (defined as bias at a luminance of 1 cd/m^2) and a maximum luminance of 5587 cd/m^2 (at 12 V). The peak external quantum and luminous efficiencies, without device optimization, are 3.9% and 8.0 cd/A, respectively. Though quantum efficiency roll-off, attributed to triplet−triplet annihilation, is observed at high current density, the efficiency remains still more than 80% (corresponding to 3.4% and 6.9 cd/A) at a benchmark luminance of 500 cd/m^2. However, it has to be noted that results with PLEDs give poorer performance as compared to devices made by vacuum thermal deposition. We therefore built up multilayered device structure by vacuum sublimation for the bluer emitter, ***fac*-6**.

For the OLEDs, four types of devices were made in total using this emitter. Two devices (devices I and II) were fabricated with the following configuration, differing only in the host used: ITO/Plexcore (25 nm)/TAPC (30 nm)/*Host*:***fac*-6** (11%) (10 nm)/BmPyPB (40 nm)/Cs_2CO_3 (1 nm)/Al (100 nm) where for device I, Host = UGH2 and for device II, Host =26DCzPPy. Device III configuration consisted of ITO/Plexcore (25 nm)/TAPC (25 nm)/26DCzPPy (5 nm)/UGH2:***fac*-6** (11%) (10 nm)/BmPyPB (40 nm)/Cs_2CO_3 (1 nm)/Al (100 nm), while the configuration of device IV can be represented as follows: ITO/Plexcore (25 nm)/TAPC (30 nm)/26DCzPPy:***fac*-6** (6%) (10 nm)/UGH2:***fac*-6** (11%) (5 nm)/BmPyPB (40 nm)/Cs_2CO_3 (1 nm)/Al (100 nm). In this stack, the dual-emissive layer has the aim of improving efficiencies by localizing the recombination zone and exciton formation at the interface between the two EMLs.

The performances of the devices are summarized in Table 6. Electroluminescent (EL) spectra plotted in Figure 7 show for

Table 6. Performances of Vacuum-Deposited Devices Containing *fac*-6

	V_{on}[a] [V]	$\eta_{ext,max}$[b] [%]	$\eta_{c,max}$[b] [cd/A]	$\eta_{p,max}$[b] [lm/W]	$CIE_{x,y}$[c]
device I	3.7	4.3	8.8	6.9	(0.16; 0.28)
device II	3.1	6.5	13.5	12.1	(0.19; 0.34)
device III	4	5.9	10.7	7.3	(0.15; 0.28)
device IV	4.2	5.8	11	7.4	(0.16; 0.29)

[a]Recorded at 1 cd/m^2. [b]η_{ext}: External quantum efficiency. η_c: Luminous efficiency. η_p: Power efficiency. [c]Recorded at 100 cd/m^2.

devices I, III, and IV a main peak at 460 nm with a less intense shoulder around 488 nm, while for device II the main peak is slightly red shifted around 465 nm with a shoulder centered at

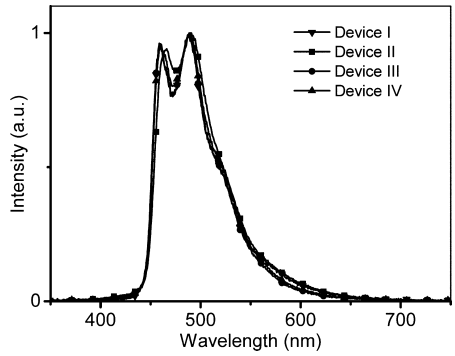

Figure 7. Electroluminescent spectra of devices I–IV.

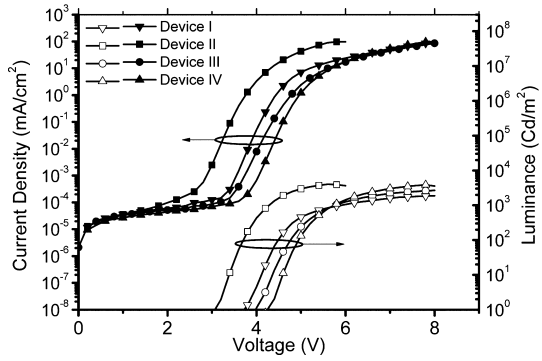

Figure 8. Current density−voltage −Luminance (I−V−L) plots of devices I–IV.

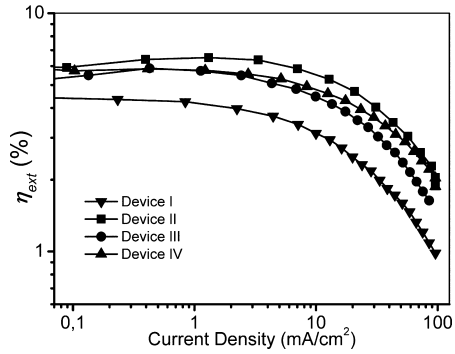

Figure 9. External quantum efficiency plots of devices I–IV.

490 nm. CIE coordinates calculated for devices I, II, and IV are all around (0.15, 0.28), while those of device III are (0.19, 0.34) due to its slightly red shifted spectra. Figures 8 and 9 show current−voltage−luminance (I−V−L) plots and external quantum efficiency (η_{ext}) plots, respectively. The impact of using a host with a wide energy band gap (UGH2) can be clearly seen by comparing devices I and II where the turn-on voltage for device I is 0.6 V higher, likely due to the more difficult charge injection into the EML. Device II shows the highest efficiency, reaching maximum external quantum efficiency, current efficiency, and power efficiency of 6.5%, 13.5 cd/A, and 12.1 lm/W, respectively. Adding an additional layer of 26DCzPPy between TAPC and the EML, i.e., going from device I to device III, raises the efficiencies from η_{ext} = 4.3% to η_{ext} = 5.9% as well as improve the luminous efficiency to 10.7 cd/A and the power efficiencies to 7.3 lm/W (Table 6). The enhancement in performance suggests that hole

dx.doi.org/10.1021/ic3018419 | *Inorg. Chem.* 2013, 52, 1812−1824

injection into the EML as well as device charge balance are improved. Having a dual-emissive layer (device IV) improves only slightly the performances, which could indicate that for UGH2-based devices charge balance was already close to optimum in device III.

CONCLUSIONS

A family of blue- and blue-green-emitting neutral bis- and tris-cyclometalated Ir(III) complexes based on 1-benzyl-4-(2,6-difluorophenyl)-1*H*-1,2,3-triazole (dfptrBn) as cyclometalating ligand has been reported and their photophysical properties investigated. The bis-cyclometalated complex **2** exhibits a marked solvatochromic behavior due to the strong MLCT character of its emissive excited state. A true blue emitter was obtained when 2-(5-(perfluorophenyl)-2*H*-1,2,4-triazol-3-yl)-pyridine (pytrF5) was used as ancillary ligand. The homoleptic complex ***fac*-4** is emissive at 77 K, showing a deep-blue emission, but it is not luminescent in solution at room temperature. The heteroleptic tris-cyclometalated complexes, with mixed arylpyridine/aryltriazole ligands, ***fac*-5** and ***fac*-6,** are highly emissive in solution and thin films, with emission colors in the blue to blue-green region. In both cases, the emission is blue shifted compared to the homoleptic arylpyridine Ir(III) counterparts. Furthermore, fluorination of the ppy ligand in ***fac*-6** increases the HOMO−LUMO gap and a blue shift of the emission is observed compared with ***fac*-5**. We rationalized the photophysical and electrochemical properties of the complexes under study by means of DFT calculations. We obtained an overall good agreement with the experimental data and the expectations for the band assignment. Due to the high emission quantum yield of complexes ***fac*-5** and ***fac*-6** we employed them as dopants in electroluminescent devices. Interestingly, for the polymer-based devices complex ***fac*-6** compared in the same conditions with FIrpic presents a very similar or even better performance than the standard blue emitter with a similar CIE.

ASSOCIATED CONTENT

Supporting Information

X-ray crystallographic data file (CIF), crystal data, and structure refinement parameters for complexes **2** and ***fac*-5**; DFT-calculated distances of the representative bonds involving the iridium atom in the ground-state geometry of complexes **2** and ***fac*-5**; table with comparison of the experimental and simulated absorption spectra features for complexes **2**, **3**, ***fac*-4**, ***fac*-5**, and ***fac*-6**; emission spectra of complex **2** in different solvents; comparison of emission spectra of complexes ***fac*-5** and ***fac*-6** in solution, neat film, and 10 wt % PMMA films; EL spectra of ***fac*-5** and ***fac*-6** at different driving voltages. This material is available free of charge via the Internet at http://pubs.acs.org.

AUTHOR INFORMATION

Corresponding Author

*E-mail: decola@uni-muenster.de, decola@unistra.fr (L.D.C.); Jerome.Cornil@umons.ac.be (J.C.); jfern_01@uni-muenster.de (J.M.F.-H.).

Present Address

[⊥]Institut de Science et d'Ingénierie Supramoléculaires (I.S.I.S.), Université de Strasbourg, 8 allée Gaspard Monge, 67000 Strasbourg, France.

Notes

The authors declare no competing financial interest.

ACKNOWLEDGMENTS

J.M.F.-H. and M.D.G.-L. would like to acknowledge Fundación Séneca (Agencia Regional de Investigación, Región de Murcia) and Ministerio de Ciencia e Innovacion, respectively, for a grant. C.-H.C. thanks the NSC and DAAD Sandwich Program for financial support. The work in Mons is supported by the Belgian National Fund for Scientific Research (FNRS). This research used resources of the Interuniversity Scientific Computing Facility located at the University of Namur, Belgium, which is supported by the F.R.S.-FNRS under convention No. 2.4617.07. J.C. is a senior research associate of FNRS.

REFERENCES

(1) Yersin, H. *Highly Efficient OLEDs with Phosphorescent Materials*; Wiley-VCH: Weinheim, 2008.
(2) Baldo, M. A.; O'Brien, D. F.; You, Y.; Shoustikov, A.; Sibley, S.; Thompson, M. E.; Forrest, S. R. *Nature* **1998**, *395*, 151−154.
(3) He, L.; Qiao, J.; Duan, L.; Dong, G. F.; Zhang, D. Q.; Wang, L. D.; Qiu, Y. *Adv. Funct. Mater.* **2009**, *19*, 2950−2960.
(4) Ulbricht, C.; Beyer, B.; Friebe, C.; Winter, A.; Schubert, U. S. *Adv. Mater.* **2009**, *21*, 4418−4441.
(5) Duan, L. A.; Hou, L. D.; Lee, T. W.; Qiao, J. A.; Zhang, D. Q.; Dong, G. F.; Wang, L. D.; Qiu, Y. *J. Mater. Chem.* **2010**, *20*, 6392−6407.
(6) Kamtekar, K. T.; Monkman, A. P.; Bryce, M. R. *Adv. Mater.* **2010**, *22*, 572−582.
(7) Xiao, L. X.; Chen, Z. J.; Qu, B.; Luo, J. X.; Kong, S.; Gong, Q. H.; Kido, J. J. *Adv. Mater.* **2011**, *23*, 926−952.
(8) Farinola, G. M.; Ragni, R. *Chem. Soc. Rev.* **2011**, *40*, 3467−3482.
(9) Zhou, G.; Wong, W.-Y.; Suo, S. *J. Photochem. Photobiol. C: Photochem. Rev.* **2011**, *11*, 133−156.
(10) Chi, Y.; Chou, P. T. *Chem. Soc. Rev.* **2007**, *36*, 1421−1431.
(11) Chi, Y.; Chou, P. T. *Chem. Soc. Rev.* **2010**, *39*, 638−655.
(12) Lee, T. C.; Hung, J. Y.; Chi, Y.; Cheng, Y. M.; Lee, G. H.; Chou, P. T.; Chen, C. C.; Chang, C. H.; Wu, C. C. *Adv. Funct. Mater.* **2009**, *19*, 2639−2647.
(13) Brooks, J.; Babayan, Y.; Lamansky, S.; Djurovich, P. I.; Tsyba, I.; Bau, R.; Thompson, M. E. *Inorg. Chem.* **2002**, *41*, 3055−3066.
(14) Vezzu, D. A. K.; Deaton, J. C.; Jones, J. S.; Bartolotti, L.; Harris, C. F.; Marchetti, A. P.; Kondakova, M.; Pike, R. D.; Huo, S. *Inorg. Chem.* **2010**, *49*, 5107−5119.
(15) Zhou, G. J.; Wong, W. Y.; Yang, X. L. *Chem.—Asian J.* **2011**, *6*, 1706−1727.
(16) Wang, Z. B.; Helander, M. G.; Hudson, Z. M.; Qiu, J.; Wang, S.; Lu, Z. H. *Appl. Phys. Lett.* **2011**, *98*, 213301.
(17) Mydlak, M.; Mauro, M.; Polo, F.; Felicetti, M.; Leonhardt, J.; Diener, G.; De Cola, L.; Strassert, C. A. *Chem. Mater.* **2011**, *23*, 3659−3667.
(18) Strassert, C. A.; Chien, C. H.; Lopez, M. D. G.; Kourkoulos, D.; Hertel, D.; Meerholz, K.; De Cola, L. *Angew. Chem., Int. Ed.* **2011**, *50*, 946−950.
(19) Zhang, Q. S.; Zhou, Q. G.; Cheng, Y. X.; Wang, L. X.; Ma, D. G.; Jing, X. B.; Wang, F. S. *Adv. Mater.* **2004**, *16*, 432.
(20) Zhang, Q. S.; Zhou, Q. G.; Cheng, Y. X.; Wang, L. X.; Ma, D. G.; Jing, X. B.; Wang, F. S. *Adv. Funct. Mater.* **2006**, *16*, 1203−1208.
(21) Armaroli, N.; Accorsi, G.; Holler, M.; Moudam, O.; Nierengarten, J. F.; Zhou, Z.; Wegh, R. T.; Welter, R. *Adv. Mater.* **2006**, *18*, 1313−1316.
(22) Armaroli, N.; Accorsi, G.; Cardinali, F. o.; Listorti, A. Photochemistry and Photophysics of Coordination Compounds: Copper. In *Photochemistry and Photophysics of Coordination Compounds I*; Springer Berlin Heidelberg: Berlin, Heidelberg, 2007; Vol. *280*, pp 69−115.
(23) Moudam, O.; Kaeser, A.; Delavaux-Nicot, B.; Duhayon, C.; Holler, M.; Accorsi, G.; Armaroli, N.; Seguy, I.; Navarro, J.; Destruel, P.; Nierengarten, J.-F. *Chem. Commun.* **2007**, 3077−3079.

(24) Zhang, L.; Li, B.; Su, Z. *J. Phys. Chem. C* **2009**, *113*, 13968−13973.
(25) Czerwieniec, R.; Yu, J.; Yersin, H. *Inorg. Chem.* **2011**, *50*, 8293−8301.
(26) Tsuboyama, A.; Iwawaki, H.; Furugori, M.; Mukaide, T.; Kamatani, J.; Igawa, S.; Moriyama, T.; Miura, S.; Takiguchi, T.; Okada, S.; Hoshino, M.; Ueno, K. *J. Am. Chem. Soc.* **2003**, *125*, 12971−12979.
(27) Deaton, J. C.; Young, R. H.; Lenhard, J. R.; Rajeswaran, M.; Huo, S. Q. *Inorg. Chem.* **2010**, *49*, 9151−9161.
(28) Thompson, M. E.; Djurovich, P. E.; Barlow, S.; Marder, S. Organometallic Complexes for Optoelectronic Applications. In *Comprehensive Organometallic Chemistry III*; Elsevier: Oxford, 2007; Vol. *12*, pp 101−194.
(29) Flamigni, L.; Barbieri, A.; Sabatini, C.; Ventura, B.; Barigelletti, F. *Top. Curr. Chem.* **2007**, *281*, 143−203.
(30) Yersin, H.; Rausch, A. F.; Czerwieniec, R.; Hofbeck, T.; Fischer, T. *Coord. Chem. Rev.* **2011**, *255*, 2622−2652.
(31) Adachi, C.; Baldo, M. A.; Thompson, M. E.; Forrest, S. R. *J. Appl. Phys.* **2001**, *90*, 5048−5051.
(32) You, Y.; Park, S. Y. *Dalton Trans.* **2009**, 1267−1282.
(33) Holmes, R. J.; Forrest, S. R.; Sajoto, T.; Tamayo, A.; Djurovich, P. I.; Thompson, M. E.; Brooks, J.; Tung, Y. J.; D'Andrade, B. W.; Weaver, M. S.; Kwong, R. C.; Brown, J. J. *Appl. Phys. Lett.* **2005**, *87*, 243507.
(34) Sajoto, T.; Djurovich, P. I.; Tamayo, A.; Yousufuddin, M.; Bau, R.; Thompson, M. E.; Holmes, R. J.; Forrest, S. R. *Inorg. Chem.* **2005**, *44*, 7992−8003.
(35) Yang, C.-H.; Cheng, Y.-M.; Chi, Y.; Hsu, C.-J.; Fang, F.-C.; Wong, K.-T.; Chou, P.-T.; Chang, C.-H.; Tsai, M.-H.; Wu, C.-C. *Angew. Chem., Int. Ed.* **2007**, *46*, 2418−2421.
(36) Sajoto, T.; Djurovich, P. I.; Tamayo, A. B.; Oxgaard, J.; Goddard, W. A.; Thompson, M. E. *J. Am. Chem. Soc.* **2009**, *131*, 9813−9822.
(37) Tamayo, A. B.; Alleyne, B. D.; Djurovich, P. I.; Lamansky, S.; Tsyba, I.; Ho, N. N.; Bau, R.; Thompson, M. E. *J. Am. Chem. Soc.* **2003**, *125*, 7377−7387.
(38) Dedeian, K.; Shi, J. M.; Shepherd, N.; Forsythe, E.; Morton, D. C. *Inorg. Chem.* **2005**, *44*, 4445−4447.
(39) Tamayo, A. B.; Garon, S.; Sajoto, T.; Djurovich, P. I.; Tsyba, I. M.; Bau, R.; Thompson, M. E. *Inorg. Chem.* **2005**, *44*, 8723−8732.
(40) Yang, C.-H.; Li, S.-W.; Chi, Y.; Cheng, Y.-M.; Yeh, Y.-S.; Chou, P.-T.; Lee, G.-H.; Wang, C.-H.; Shu, C.-F. *Inorg. Chem.* **2005**, *44*, 7770−7780.
(41) Chien, C.-H.; Fujita, S.; Yamoto, S.; Hara, T.; Yamagata, T.; Watanabe, M.; Mashima, K. *Dalton Trans.* **2008**, 916−923.
(42) Chang, C.-F.; Cheng, Y.-M.; Chi, Y.; Chiu, Y.-C.; Lin, C.-C.; Lee, G.-H.; Chou, P.-T.; Chen, C.-C.; Chang, C.-H.; Wu, C.-C. *Angew. Chem., Int. Ed.* **2008**, *47*, 4542−4545.
(43) Haneder, S.; Da Como, E.; Feldmann, J.; Lupton, J. M.; Lennartz, C.; Erk, P.; Fuchs, E.; Molt, O.; Münster, I.; Schildknecht, C.; Wagenblast, G. *Adv. Mater.* **2008**, *20*, 3325−3330.
(44) Sasabe, H.; Takamatsu, J.; Motoyama, T.; Watanabe, S.; Wagenblast, G.; Langer, N.; Molt, O.; Fuchs, E.; Lennartz, C.; Kido, J. *Adv. Mater.* **2010**, *22*, 5003−5007.
(45) Lo, S.-C.; Shipley, C. P.; Bera, R. N.; Harding, R. E.; Cowley, A. R.; Burn, P. L.; Samuel, I. D. W. *Chem. Mater.* **2006**, *18*, 5119−5129.
(46) Lai, W.-Y.; Levell, J. W.; Jackson, A. C.; Lo, S.-C.; Bernhardt, P. V.; Samuel, I. D. W.; Burn, P. L. *Macromolecules* **2010**, *43*, 6986−6994.
(47) Kolb, H. C.; Finn, M. G.; Sharpless, K. B. *Angew. Chem., Int. Ed.* **2001**, *40*, 2004−2021.
(48) Finn, M. G.; Kolb, H. C.; Fokin, V. V.; Sharpless, K. B. *Prog. Chem.* **2008**, *20*, 1−4.
(49) Beyer, B.; Ulbricht, C.; Escudero, D.; Friebe, C.; Winter, A.; Gonzalez, L.; Schubert, U. S. *Organometallics* **2009**, *28*, 5478−5488.
(50) Felici, M.; Contreras-Carballada, P.; Smits, J. M. M.; Nolte, R. J. M.; Williams, R. M.; De Cola, L.; Feiters, M. C. *Molecules* **2010**, *15*, 2039−2059.
(51) Fernandez-Hernandez, J. M.; Yang, C.-H.; Beltran, J. I.; Lemaur, V.; Polo, F.; Fröhlich, R.; Cornil, J.; De Cola, L. *J. Am. Chem. Soc.* **2011**, *133*, 10543−10558.
(52) Botelho, M. B. S.; Fernandez-Hernandez, J. M.; de Queiroz, T. B.; Eckert, H.; De Cola, L.; de Camargo, A. S. S. *J. Mater. Chem.* **2011**, *21*, 8829−8834.
(53) Ladouceur, S.; Fortin, D.; Zysman-Colman, E. *Inorg. Chem.* **2011**, *50*, 11514−11526.
(54) You, Y. M.; Park, S. Y. *J. Am. Chem. Soc.* **2005**, *127*, 12438−12439.
(55) Orselli, E.; Kottas, G. S.; Konradsson, A. E.; Coppo, P.; Frohlich, R.; Frtshlich, R.; De Cola, L.; van Dijken, A.; Buchel, M.; Borner, H. *Inorg. Chem.* **2007**, *46*, 11082−11093.
(56) Baranoff, E.; Curchod, B. F. E.; Monti, F.; Steimer, F.; Accorsi, G.; Tavernelli, I.; Rothlisberger, U.; Scopelliti, R.; Grätzel, M.; Nazeeruddin, M. K. *Inorg. Chem.* **2012**, *51*, 799−811.
(57) Wang, Z.-X.; Zhao, Z.-G. *J. Heterocycl. Chem.* **2007**, *44*, 89−92.
(58) Otwinowski, Z.; Minor, W. *Methods Enzymol.* **1997**, *276*, 307−326.
(59) Otwinowski, Z.; Borek, D.; Majewski, W.; Minor, W. *Acta Crystallogr., Sect. A* **2003**, *59*, 228−234.
(60) Sheldrick, G. M. *Acta Crystallogr., Sect. A* **1990**, *46*, 467−473.
(61) Sheldrick, G. M. *Acta Crystallogr., Sect. A* **2008**, *64*, 112−122.
(62) Antonello, S.; Musumeci, M.; Wayner, D. D. M.; Maran, F. *J. Am. Chem. Soc.* **1997**, *119*, 9541−9549.
(63) Lee, C. T.; Yang, W. T.; Parr, R. G. *Phys. Rev. B* **1988**, *37*, 785−789.
(64) Curtiss, L. A.; Redfern, P. C.; Raghavachari, K.; Pople, J. A. *J. Chem. Phys.* **2001**, *114*, 108−117.
(65) Chiodo, S.; Russo, N.; Sicilia, E. *J. Chem. Phys.* **2006**, *125*, 104107.
(66) Avilov, I.; Minoofar, P.; Cornil, J.; De Cola, L. *J. Am. Chem. Soc.* **2007**, *129*, 8247−8258.
(67) Yang, C. H.; Beltran, J.; Lemaur, V.; Cornil, J.; Hartmann, D.; Sarfert, W.; Frohlich, R.; Bizzarri, C.; De Cola, L. *Inorg. Chem.* **2010**, *49*, 9891−9901.
(68) Xu, M.-L.; Che, G.-B.; Li, X.-Y.; Xiao, Q. *Acta Crystallogr., Sect. E* **2009**, *65*, m28.
(69) Berger, R. J. F.; Stammler, H.-G.; Neumann, B.; Mitzel, N. W. *Eur. J. Inorg. Chem.* **2010**, *11*, 1613−1617.
(70) Tamao, K.; Uchida, M.; Izumizawa, T.; Furukawa, K.; Yamaguchi, S. *J. Am. Chem. Soc.* **1996**, *118*, 11974−11975.
(71) Orselli, E.; Albuquerque, R. Q.; Fransen, P. M.; Frohlich, R.; Janssen, H. M.; De Cola, L. *J. Mater. Chem.* **2008**, *18*, 4579−4590.
(72) Treboux, G.; Mizukami, J.; Yabe, M.; Nakamura, S. *Chem. Lett.* **2007**, *36*, 1344−1345.
(73) Bard, A. J.; Faulkner, L. R. *Electrochemical Methods, Fundamentals and Applications*, 2nd ed.; Wiley: New York, 2001.
(74) Thelakkat, M.; Schmidt, H.-W. *Adv. Mater.* **1998**, *10*, 219−220.